SCIENCE CHINA
Information Sciences

June 2020, Vol. 63 160402:1–160402:8
https://doi.org/10.1007/s11432-019-2837-0

• REVIEW •
Special Focus on Photonics in AI

A brief review of integrated and passive photonic reservoir computing systems and an approach for achieving extra non-linearity in passive devices

Dachuan WU[1], Yasha YI[1,2*] & Yuxiao ZHANG[1]

[1]*Integrated Nano Optoelectronics Laboratory, Department of Electrical and Computer Engineering, University of Michigan, Dearborn* 48128*, USA;*
[2]*Energy Institute, University of Michigan, Ann Arbor* 48109*, USA*

Received 3 December 2019/Revised 12 February 2020/Accepted 12 March 2020/Published online 13 May 2020

Abstract Photonic-based reservoir computing (RC) systems have attracted significant attention. Integrated and purely passive systems are compatible with complementary metal-oxide-semiconductor devices, but are limited by the lack of non-linear components. This study consists of two parts: firstly, a review on the published integrated and passive RC system is presented. The review focuses on the structural configuration (rather than the mathematical model) of the neural network; secondly, a new approach for achieving an integrated and passive photonic RC system is introduced and discussed. This approach employs a mode combiner in front of the reservoir to achieve an extra non-linearity in a purely passive device. Moreover, the approach is numerically investigated, and an XOR (exclusive or) task is used to test the device, and the result shows that the new approach satisfies the requirement of an RC system.

Keywords reservoir computing, integrated photonics, neural network, non-linearity

Citation Wu D C, Yi Y S, Zhang Y X. A brief review of integrated and passive photonic reservoir computing systems and an approach for achieving extra non-linearity in passive devices. Sci China Inf Sci, 2020, 63(6): 160402, https://doi.org/10.1007/s11432-019-2837-0

1 Introduction

In recent years, significant progress has been made in the field of artificial neural networks. Reservoir computing (RC), which is a type of recurrent neural network (RNN), has also been widely studied, owing to its easy training process [1, 2]. Compared with a traditional RNN, an RC system consists of an extra readout layer where the readout weights will be trained. The hidden layers (referred to as the reservoir) of the original RNN are left untrained. Therefore, the training process in an RC system applies to only one layer (rather than every layer as in the case of a traditional RNN), leading to significant reduction in the time and energy consumption.

Similar to the other types of artificial neural networks, the initial proposed RC systems were also considered to be based on software. However, the software relies on the computer hardware and thus, relies on the transistor-based electronic devices. The time and energy consumption of a software RC system is therefore limited by these devices. Compared with the traditional RNN, an RC system is characterized by lower time and energy consumption and hence, further overcoming the hardware limitations is also essential to improve these systems.

* Corresponding author (email: yashayi@umich.edu)

Considerable effort has been expended in realizing RC systems by employing different types of hardware including electronic, photonic, mechanical, or biological systems. A review of the efforts expended up to mid-2018 is presented in [3]. Among the aforementioned hardware systems, the photonic system is unique, owing to its ultra-high calculation speed and ultra-low power consumption associated with the propagation nature of photons. In [3], the study of photonic RC is classified into two groups, i.e., studies considering spatial node systems and studies considering temporal node systems. This classification refers to the approach for achieving multiple nodes. However, these studies can also be classified based on the fabrication method of the systems. This classification considers the industrial feasibility of the system, i.e., the fabrication method is directly related to commercialization of the system. Therefore, all the photonic RC systems can be classified by two standards: firstly, is the system integrated or based on free-space optics? Secondly, is the system passive or active?

From the viewpoint of fabrication, the integrated and passive systems are the easiest to fabricate; they are usually complementary metal-oxide-semiconductor compatible and therefore, are suited for the mature microchip fabrication industry, where they can be mass-produced at a low cost. However, from the viewpoint of system performance, the passive systems are the hardest to realize because of the lack of non-linear components. This has resulted in relatively few integrated and purely passive systems, although several other photonic RC systems have been proposed.

In this study, a current review of the integrated and purely passive photonic RC systems is provided in Section 2. This review concentrates on the structural configuration, rather than mathematical models, of these systems. An approach for realizing extra non-linearity in a purely passive device is introduced and discussed in Section 3, and this approach is numerically investigated. In the structure, a mode combiner is applied prior to the reservoir, and owing to the natural square law detection of the photodetector, the readout result becomes the square of the sum of two different electrical fields.

2 Review on integrated and purely passive photonic RC systems

As previously stated, studies on integrated and purely passive photonic RC systems are rare, owing mainly to the lack of non-linear components. An integrated and passive photonic device is usually fabricated on a Si wafer. However, Si has an indirect bandgap and hence, the performance of Si-based active components (such as an on-chip light source or a detector) is usually inferior to that of the III–V-based components. As a result, in the limited studies about integrated and passive RC systems, the non-linearity relies entirely on the detector; the light has to be detected to become a readout, and the natural square law detection of the electrical field can generate the non-linearity. Based on this theory, the studies using free-space optics or active phenomena such as semiconductor optical amplifier or two photon absorption are excluded from this review.

To the best of our knowledge, most of these systems are proposed by the photonic research group at Ghent University [4–13]. Their studies utilize the spatial node scheme: the reservoir contains one or more input ports but multiple output ports. When input is entered into the system, different intensities can be detected from each output port, and the number of output ports is the number of nodes in the readout layer. In [4], a 16 node system is experimentally investigated (see Figure 1(a) for the structural configuration). In this system, delay lines and 1×2 or 2×2 multimode interferometers are used to connect every node and induce the recurrent effect, and a grating coupler is used for input and readout. The input signal is entered into the system from one node, and all 16 nodes are detected for the readout. The training is done offline after the detection. The system contains no single active element and hence, the non-linearity relies entirely on the square law of the detector. Three types of tasks, including 2-bit XOR (exclusive or) logical operation, header recognition, and spoken digit classification, are demonstrated. In this system, very long delay lines are required to ensure that the recurrent effect is induced at the right time. However, this also leads to considerable optical propagation loss, with only 11 of the 16 nodes offering intensity higher than the noise level (see Figure 1(a)). The input node is indicated by an arrow in the figure, and the 11 red nodes are characterized by readable intensity.

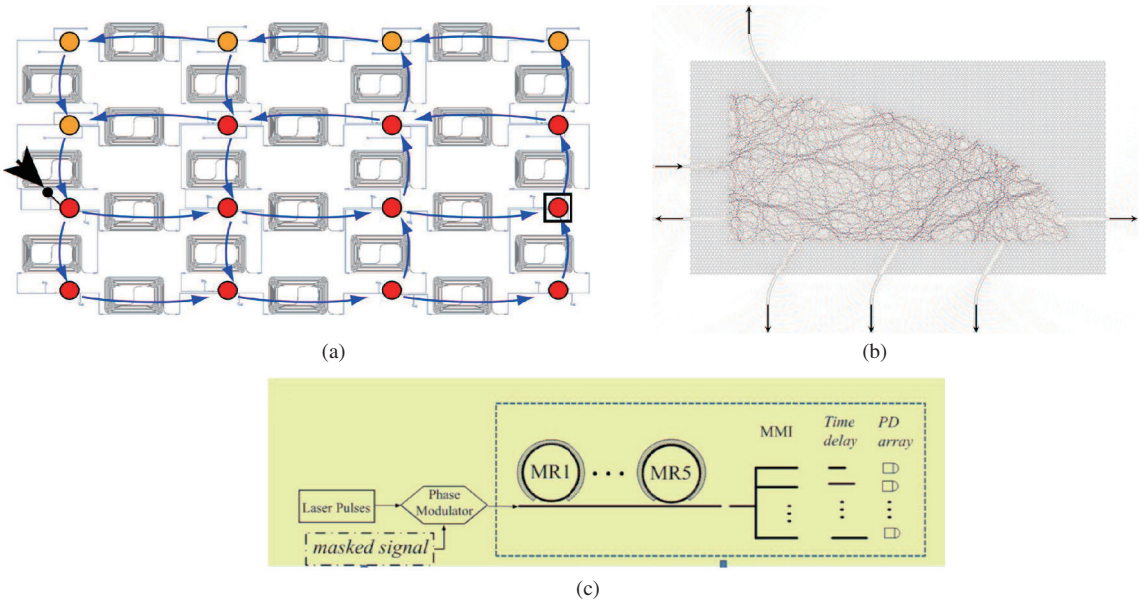

Figure 1 (Color online) Illustration showing different structure types of integrated and passive RC systems. (a) 16 nodes, spatial node system (from [4]); (b) photonic crystal cavity with seven defects, spatial node system (from [9]); (c) time-delay effect induced by cascaded ring resonators, temporal node system (from [14]).

This intensity issue results from two factors: a single input and a high propagation loss, and can be addressed by considering both factors [5–7]. In [5], a multi-input strategy was numerically investigated, as further summarized in [6]. The results revealed that in the 16-node system, the optimal performance is achieved if the input is sent to all the nodes. However, an optimized 4-node input strategy can achieve an equivalent performance. In [7], the multimode interferometer is carefully optimized to suppress the insertion loss and hence, the total propagation loss is reduced.

Other studies have focused on photonic crystals [8, 9]. In [8], a photonic crystal waveguide with a designed cavity is used to generate periodic patterns, and a waveform prediction task is realized in this system. In [9], a large photonic crystal cavity with seven defects is used as the reservoir, where one of the defects was used as input and the other six are used as readout nodes. Figure 1(b) shows the structure of the present study, the light propagation mechanism inside the cavity is left as a black box in some extent.

Several related studies have also been performed by the Ghent group [10–13]. In [10], a method for efficiently simulating the optical cavity is proposed. Ref. [11] used a digital mask to address another issue in the integrated RC system; if the system is overly compact, the optical time delay will be short, thereby requiring an overly rapid input and readout rates that are impractical for real applications. Ref. [12] reported that the on-chip integrated RC system can handle various tasks. In their most recent study [13], an all-optical readout strategy is considered and realized, and elimination of opto-electronic readout schemes resulted in further reduction of the power consumption.

In addition to the spatial node scheme, the temporal node scheme can also be used to design an RC system. This type of system contains a reservoir with only one output exit, and multiple numbers of readout nodes are achieved by the time delay; multiple detections within the time interval of an input digit can be obtained, and the intensity may differ among the detections, leading to a temporal distribution of the readout nodes. To the best of our knowledge, only one study [14] uses this scheme on an integrated and passive system. In [14], five cascaded ring resonators are used as the reservoir, and the single pulse in the time domain can be converted to multiple pulses, owing to the time-delay effect of the ring resonators. Some of the pulses will fall into the subsequent digit, which provides the recurrent effect to the system. The structure is shown in Figure 1(c). The input is phase-modulated before entering the reservoir, and due to the limited response time of the current photodetectors, an MMI (Mach-Zehnder interferometer) is used at the detection end to separate the output into different exits. Furthermore, the delay length

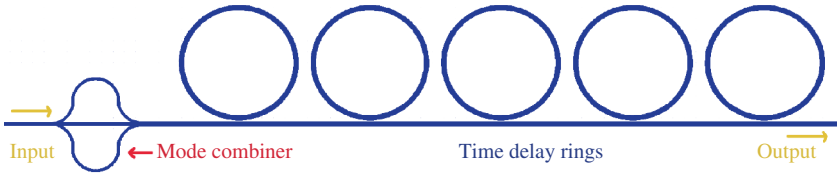

Figure 2 (Color online) Structural configuration of the device.

differs among the exits reached before the photodetector and therefore, a temporal readout resolution of this system overcomes the limitation of the photodetector response time.

3 RC system with mode combiner to achieve extra non-linearity

In our study, we follow the temporal node scheme in [14] and improve the structural level; a mode combiner is used to provide the extra non-linearity. The finite difference time domain (FDTD) method is used to verify the system. Figure 2 shows the structural configuration, and the waveguide material is considered to be Si. A material effective index of 3 and a loss of 1 dB/cm are applied to mimic the Si waveguide in the SiO_2 environment. The delay function is achieved using five cascaded ring resonators, similar to the method reported in [14]. A mode combiner is applied prior to the time-delay rings, thereby converting the TM-polarized single mode input to a combination of the TM 0th mode and the TM 1st mode. The two modes are characterized by different mode effective indices and different time-delay functions in the rings and exhibit the same polarization. As a result, when the light is detected by a photodetector at the output port, the natural square law detection applies to the sum of the electrical field associated with each mode. Therefore, the non-linearity is helped by two factors: the natural square law detection and difference between the effective indices of the two modes, where

$$I = |\boldsymbol{E}_{\mathrm{TM0}} + \boldsymbol{E}_{\mathrm{TM1}}|^2. \tag{1}$$

The recurrent effect of the device is provided by the time-delay function of the cascaded ring resonators. Compared with [14], a few adjustments are applied in this study, for ease of the simulations; firstly, the time interval for one digit input is set to 700 fs and secondly, the radius of each ring is set to 5 μm for coincidence with the one digit time interval, and the five rings are set to be exactly the same. In each digit, the intensity is set to either 1 or 0 in the whole interval and hence, the signal is non-return-to-zero. We pick 120 readouts every 5 fs in one digit at the output end. This is incompatible with present-day technology, because the response time of a common photodetector is on the order of 25 ps [14] and therefore, a readout every 5 fs is impossible. However, rather than considering adjustment of the delayed time, this study considers the extra non-linearity created by the mode combiner. Ref. [14] provided a detail explanation for the design of a realistic time-delay structure using five rings and hence, we assume that considering a readout of every 5 fs is acceptable for a proof-of-concept. In actual cases, different time intervals can be applied for one digit and therefore, the readout speed can be adjusted to the same order of the response time of a current photodetector.

The spectrum response of the ring resonators is first investigated. Figure 3 shows the output spectrum obtained for one of the resonators. In addition to the previously mentioned radius (5 μm), the width of both rings and the bus waveguide are set to 450 nm. Similarly, the gap between the rings and the waveguide is set to 100 nm. The output spectra are obtained by means of a two-dimensional FDTD simulation. The red curve shows the response of the TM 0th mode, where a resonance occurs at 1563 nm. Coincidentally, this wavelength corresponds to the resonance in the blue curve, i.e., the response of the TM 1st mode. Incomplete resonance is observed in the blue curve, and the Q-factor of the TM1 resonances is considerably lower than that of TM0. Consequently, the ring resonator will still offer a good time-delay function for both modes on this wavelength. Therefore, 1563 nm is slected as the working wavelength of the device.

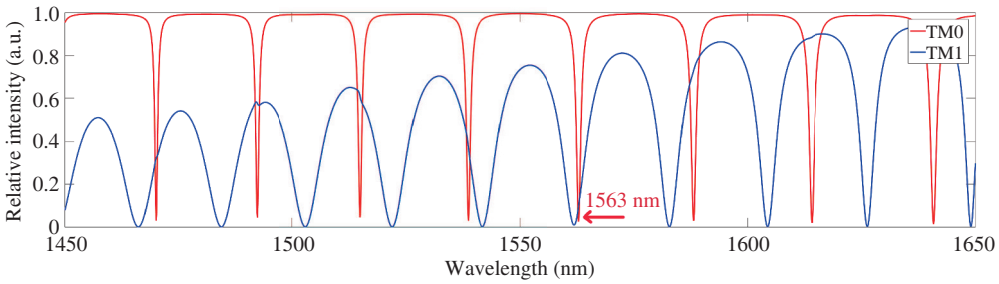

Figure 3 (Color online) Output spectrum of one ring resonator: red curve is the TM 0th mode, and blue is the TM 1st mode.

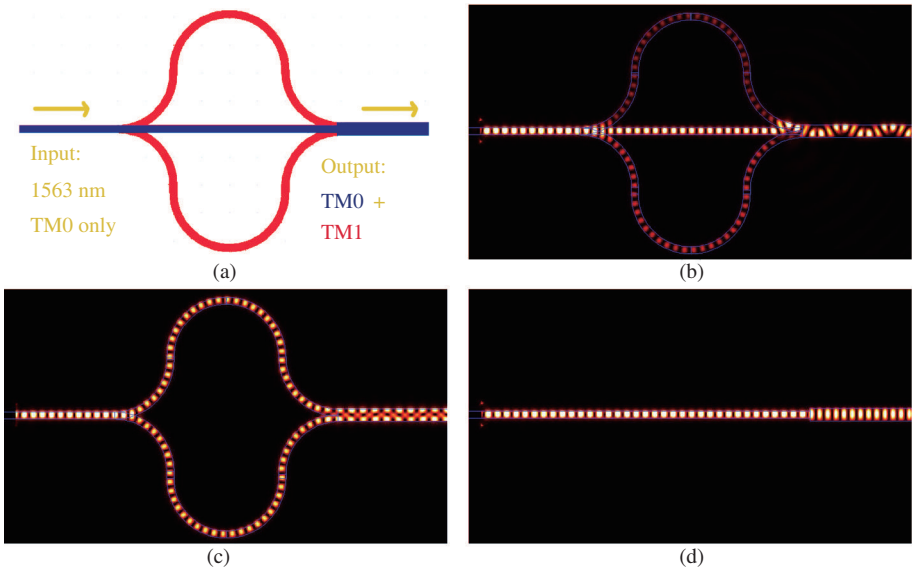

Figure 4 (Color online) The mode combiner. (a) Structure configuration, both the red and blue waveguides are Si. (b) Field distribution of the entire structure. (c) Field distribution of the red arm: TM 0th mode converted to TM 1st mode. (d) Field distribution of the blue arm: TM 0th mode is maintained.

The mode combiner is then investigated. Figure 4(a) shows an illustration of this part. The light coming from the input port is only in the TM 0th mode, because the width of the waveguide is set to only 250 nm. Nevertheless, the output waveguide is set to 450 nm, and the light will become a combination of the TM 0th mode and the TM 1st mode; the two red arms in Figure 4(a) differ slightly in length, which will result in a π phase difference. Therefore, when the two 250 nm arm are combined into a 450 nm waveguide, a TM 1st mode is generated, as evidenced by the field distribution in Figure 4(c). The blue arm in the middle will keep the light in a fundamental mode, as shown in Figure 4(d). Consequently, when all three arms are used together, the output light will become a combination: most of the light will remain in the TM 0th mode, and a small portion of the light will be converted to the TM 1st mode (see Figure 4(b) for the field distribution of the total effect). From the simulation, we find that 49.46% of the input remain in the TM 0th mode, 25.81% is converted into the TM 1st mode, and the rest (24.73% becomes the insertion loss).

The time-delay function of the two modes is also investigated (see Figure 5 for the corresponding results). In this simulation, a sinusoidal pulse of 700 fs with a central wavelength of 1563 nm is sent as the input, and the structure in Figure 1 is employed. Figure 5(a) shows the delay function when the pulse is set to the TM 0th mode. When the pulse goes through the ring resonators, part of the light couples into the ring, leading to multiple pulses in the time-delay figure; the main body of the pulse reaches the detection end with a peak time at 1150 fs. At the detection end, this pulse contributes to the readout in the same digit; the part of the light that is coupled into the rings forms the other pulses and will

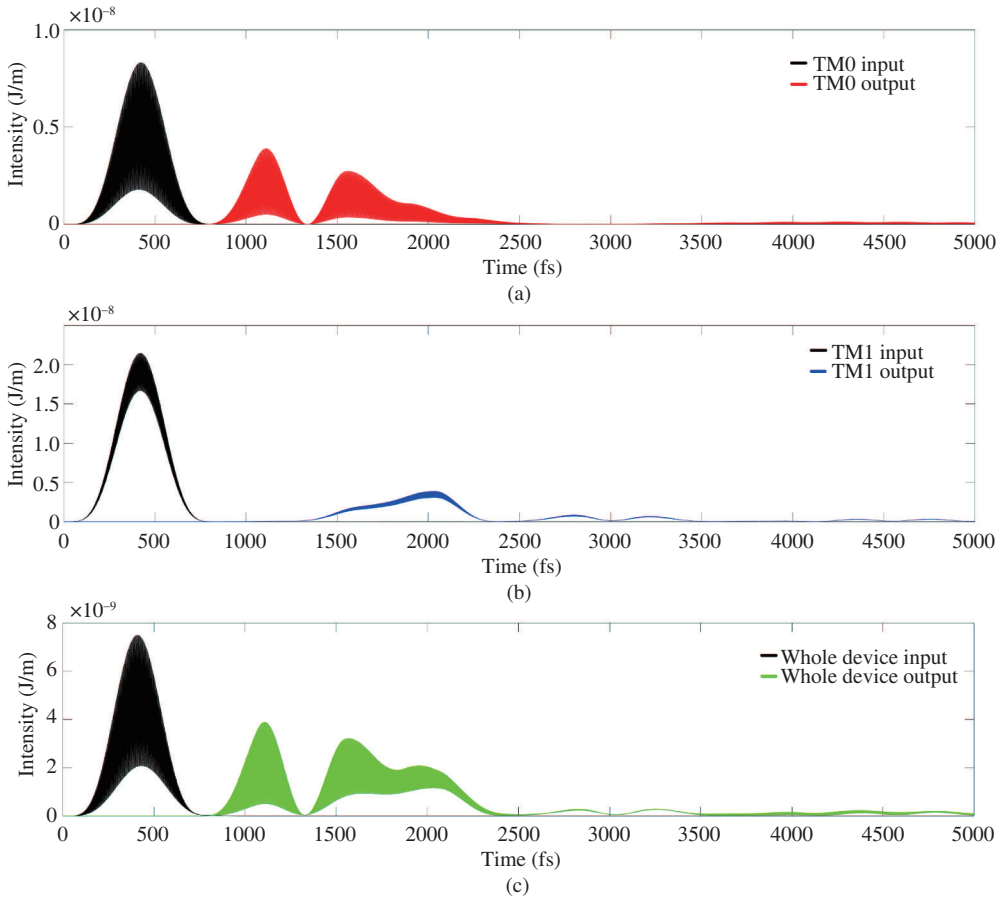

Figure 5 (Color online) Time-delay function of a single sinusoidal pulse. Delay function for the (a) TM 0th mode only, (b) TM 1st mode only, and (c) whole device with the mode combiner. Black part in each figure represents the input pulse.

contribute to the readout in the following digits. These delayed pulses exert a recurrent effect on the whole device. Figure 5(b) shows the delay function of the TM 1st mode. The pulse that is supposed to contribute to the same digit disappears completely, and all the light which goes to the pulses contributes to the recurrent effect. This is because the ring resonators form a low Q resonance on the TM 1st mode and hence, all the light couples into the rings when the input pulse goes through the rings. Figure 5(c) shows the delay function of the two modes combined; the shape of the first pulse is similar to that of the pulse shown in Figure 5(a). The first pulse is contributed entirely by the TM 0th mode. However, the other pulses are stronger than those shown in Figure 5(a), this extra part is from the TM 1st mode. This indicates that the influence of the input on the subsequent digits is enhanced by the TM 1st mode, and this enhancement results from use of the mode combiner.

In this study, the signal is coded only by the intensity modulation. We run the whole device with an input containing 100 digits of either 1 or 0, and the data is randomly selected. Figure 6 shows the simulation results; the input intensity is shown in Figure 6(a) and the output is shown in Figure 6(b). In each digit, 120 readouts are collected every 5 fs as the output nodes. The training task is set to be a simple XOR task on each digit and the previous digit.

After the simulation, the data is trained and tested using software. The first 80 digits are used for training and the last 20 digits are used for testing. The mean square error (MSE) is used to characterize the performance. The node number (120) is larger than the data number for training (80). Therefore, the bias in the ridge-regression is randomly picked at first, and is then used to find the smallest MSE in the test data (the corresponding results are shown in Figure 7). The fit between the trained data and the target is shown in Figure 7(a). Ridge-regression is used to avoid overfitting. Although we use 120 nodes to fit 80 digits of data, the fit is imperfect, but this is actually helpful for the performance. After

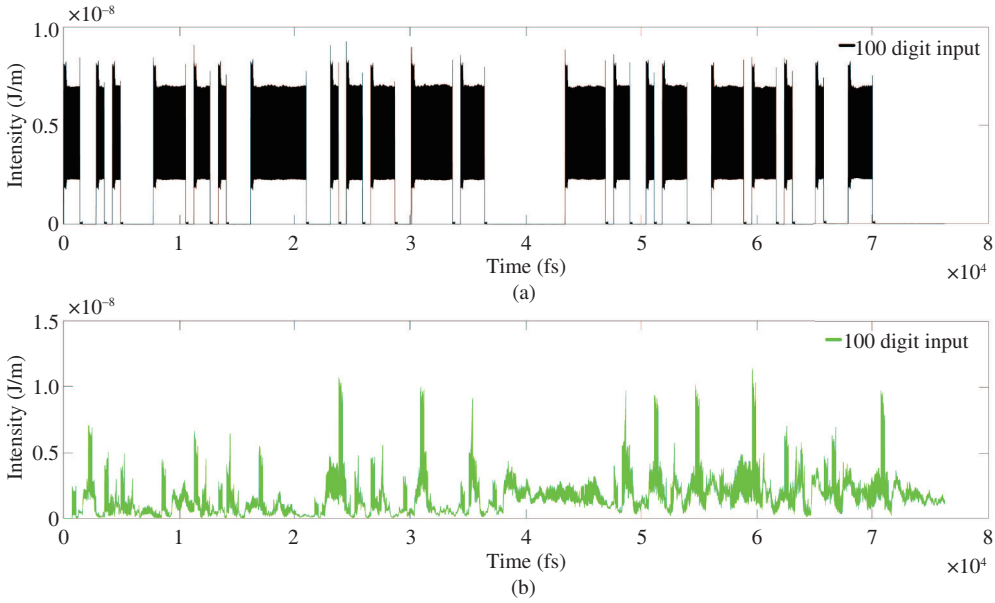

Figure 6 (Color online) Time-delay function for the 100 digit coded input. (a) Input intensity, the code is randomly selected; (b) the output response of the input.

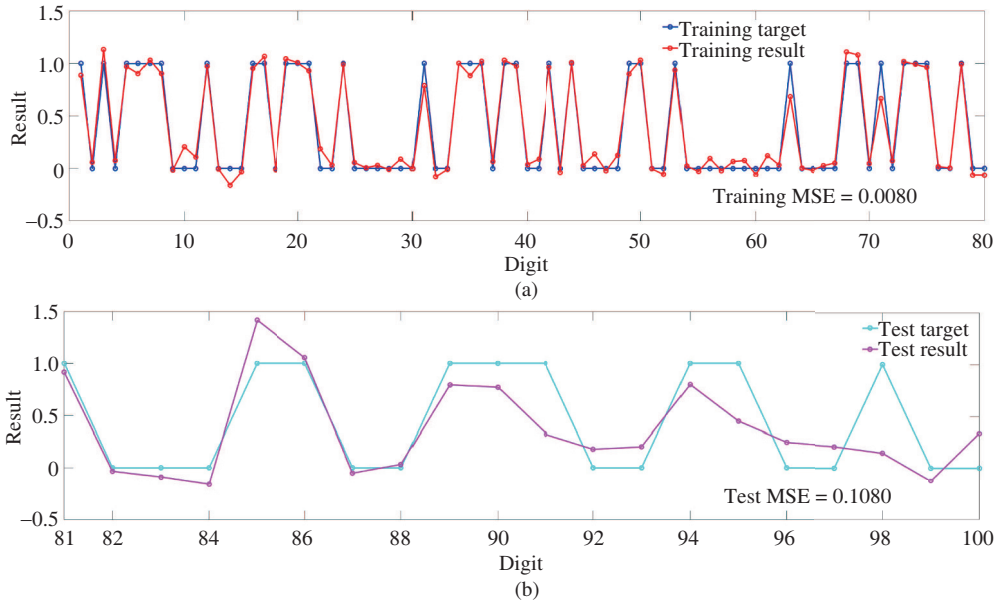

Figure 7 (Color online) Training and test results. (a) Trained data is shown by the red curve, and the blue curve shows the training target, MSE = 0.0080. (b) Test data is shown by the pink curve, and the light blue curve shows the test target, MSE = 0.1080.

training, the trained weights are tested by the test data, which is shown in Figure 7(b). The results are close to the target for most of the 20 digits, except for digits 91, 95, and 98. Considering that only 80 digits are used in the training process, this test result is satisfactory. This performance is achieved by utilizing ridge-regression with a fine-tuned bias (MSE of the test data: 0.1080, bias used: 10^{-19}).

4 Conclusion

In this study, the advantage of using integrated and passive photonic devices in RC is discussed, and the published systems in this category are reviewed with a focus on the structural configuration of these

devices. The results indicated that both spatial and temporal node schemes can be used to design an integrated and passive RC system. The non-linear function of such systems usually relies on the natural square law detection of the photodetector. Based on this knowledge, an approach for achieving extra non-linearity in passive systems is introduced and discussed. In the system, a mode combiner can be applied prior to the reservoir. The electrical field at the detection end becomes the sum of two modes with the same polarization, owing to this combiner, and both modes can contribute to the square law detection. The structure is numerically investigated, and an XOR task is employed to determine the performance. The result shows that a test MSE of 0.1080 can be achieved via ridge-regression.

Acknowledgements This work was supported by National Science Foundation (Grant No. NSF-1710885).

References

1 Jaeger H. Harnessing nonlinearity: predicting chaotic systems and saving energy in wireless communication. Science, 2004, 304: 78–80
2 Maass W, Natschläger T, Markram H. Real-time computing without stable states: a new framework for neural computation based on perturbations. Neural Comput, 2002, 14: 2531–2560
3 Tanaka G, Yamane T, Héroux J B, et al. Recent advances in physical reservoir computing: a review. Neural Netw, 2019, 115: 100–123
4 Vandoorne K, Mechet P, van Vaerenbergh T, et al. Experimental demonstration of reservoir computing on a silicon photonics chip. Nat Commun, 2014, 5: 3541
5 Katumba A, Freiberger M, Bienstman P, et al. A multiple-input strategy to efficient integrated photonic reservoir computing. Cogn Comput, 2017, 9: 307–314
6 Freiberger M, Katumba A, Bienstman P, et al. On-chip passive photonic reservoir computing with integrated optical readout. In: Proceedings of 2017 IEEE International Conference on Rebooting Computing (ICRC), 2017. 1–4
7 Katumba A, Heyvaert J, Schneider B, et al. Low-loss photonic reservoir computing with multimode photonic integrated circuits. Sci Rep, 2018, 8: 2653
8 Fiers M A A, van Vaerenbergh T, Wyffels F, et al. Nanophotonic reservoir computing with photonic crystal cavities to generate periodic patterns. IEEE Trans Neural Netw Learn Syst, 2014, 25: 344–355
9 Laporte F, Katumba A, Dambre J, et al. Numerical demonstration of neuromorphic computing with photonic crystal cavities. Opt Express, 2018, 26: 7955
10 van Vaerenbergh T, Fiers M, Dambre J, et al. Efficient simulation of optical nonlinear cavity circuits. Opt Quant Electron, 2015, 47: 1471–1476
11 Schneider B, Dambre J, Bienstman P. Using digital masks to enhance the bandwidth tolerance and improve the performance of on-chip reservoir computing systems. IEEE Trans Neural Netw Learn Syst, 2016, 27: 2748–2753
12 Katumba A, Freiberger M, Laporte F, et al. Neuromorphic computing based on silicon photonics and reservoir computing. IEEE J Sel Top Quantum Electron, 2018, 24: 1–10
13 Ma C, Sackesyn S, Dambre J, et al. All-optical readout for integrated photonic reservoir computing. In: Proceedings of 2019 21st International Conference on Transparent Optical Networks (ICTON), 2019. 1–4
14 Zhang H, Feng X, Li B, et al. Integrated photonic reservoir computing based on hierarchical time-multiplexing structure. Opt Express, 2014, 22: 31356